Plasma Physics, Vol. 23, No. 8, pp. 679 to 691, 1981.
Printed in Northern Ireland

0032-1028/81/080679-13$02.00/0
Institute of Physics and Pergamon Press Ltd.

HIGH POWER HEATING IN THE ION CYCLOTRON RANGE OF FREQUENCIES IN THE WISCONSIN TOKAPOLE II

A. P. BIDDLE and J. C. SPROTT
Department of Physics, University of Wisconsin, Madison, WI 53706, U.S.A.

(*Received* 2 *October* 1980)

Abstract—Fast wave heating at the second, third and fourth harmonics of the ion cyclotron resonance, and slow wave heating at the fundamental in a single ion species hydrogen plasma, are found to be in good agreement with warm plasma theory at rf power levels ≤130 kW. Ion heating is negligible off an eigenmode. Ion body temperatures are more than doubled to 75 eV from the 35 eV ohmically heated case with tails comprising 8% of the plasma at 320 eV. No deleterious effects except a non-disruptive 10% shortening of the discharge length caused by impurity influx are noted. A passive mode tracking technique allows ≈40% increase in power deposition in a passing eigenmode over that of a fixed frequency rf source. Ion temperatures are limited by charge exchange due to the <50 eV central temperature and the small 13 cm radius current channel.

1. INTRODUCTION

THE NEED for supplementary ion heating to achieve ignition in a Tokamak reactor is well appreciated (ROTHMAN *et al.*, 1969; HOSEA and HOOKE, 1973; VDOVIN *et al.*, 1976). The use of fast magnetosonic waves in the ion cyclotron range of frequencies to excite eigenmodes for improved power deposition has been studied (STIX, 1975; HWANG and GOULD, 1980), usually at the second harmonic of the majority deuterium species. The presence of a varying and sometimes inadvertent minority of protons has complicated the interpretation of the true harmonic heating effectiveness.

We report an ICRF experiment in the Wisconsin Tokapole II device, a Tokamak with four poloidal divertors. This device allows study of many of the facets of rf heating a Tokamak plasma with multiple poloidal divertors and a cold gas blanket in the divertor scrapeoff region. The rf mode structures are measured unambiguously with probes inserted directly into the plasma. The spatial distribution of the rf fields is determined by the current channel size and density, unaffected by the presence of the internal divertor rings.

The ion body temperature limit is consistent with charge exchange loss while the tail, a characteristic of ion cyclotron harmonic heating schemes, is limited by the low poloidal flux and the small physical size of the machine. The resultant particle loss is to the internal rings and to the antenna structure, emphasizing the need for higher plasma currents. While the best heating occurs at $\omega = 2\omega_{ci}$, significant heating occurs at the third, fourth and fifth harmonics.

2. APPARATUS AND DIAGNOSTICS

The Tokapole II device has been described in detail by BIDDLE *et al.*, (1979). Briefly, it is a Tokamak with four inductively driven internal copper field shaping rings, 5 cm in minor diameter, and a typical plasma current $I_p \approx 30$ kA with the ICRF antenna installed. The ohmic heating transformer also drives the internal ring currents. These supplementary rings behave as magnetic limiters and allow the formation of non-circular cross-sections (LIPSCHULTZ *et al.*, 1979). A poloidal

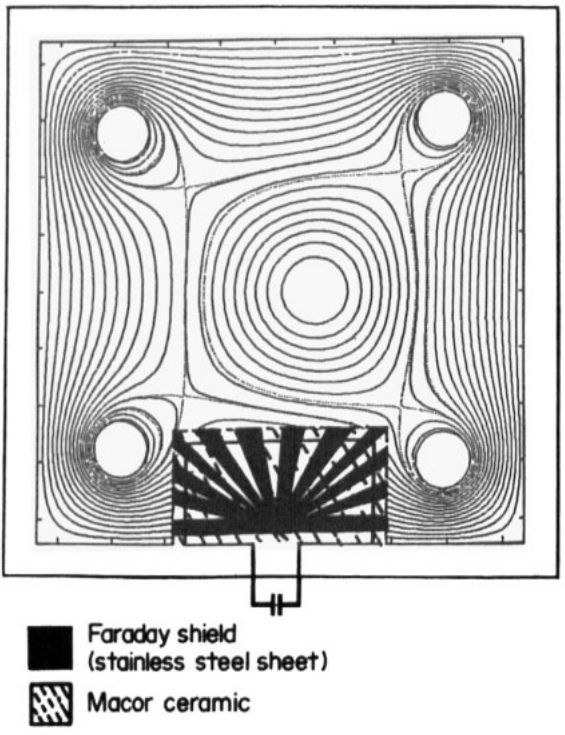

FIG. 1.—Poloidal cross-section showing poloidal flux plot with plasma current present, internal copper rings and rf launching structure.

cross section is shown in Fig. 1 which includes a typical poloidal flux plot and the physical locations of the rings and antenna. The major radius is 50 cm, and the square minor cross-section is 44 cm on a side. The toroidal field is operated derated from 8 to 4 kG in order to place the $\omega = 2\omega_{ci}$ resonance of the existing rf source on axis. The poloidal field near the ring surfaces reaches 5 kG but causes the $|B|$ surfaces to deviate significantly from the usual vertical cylinders only near the rings. Line average densities are measured using a 70 GHz interferometer. Electron temperatures are inferred by spectroscopic techniques (GROEBNER, 1979), and the ion temperature is measured by a charge exchange analyzer. It is conventional except that the stripping cell gas, N_2, is supplied by a fast puff valve. This allows a substantially higher cell pressure to be used to maximize the analyzer sensitivity while minimizing the gas loading on the pumping system and contamination of the plasma. The relatively high neutral density, $n_H \approx 5 \times 10^{11}\,\mathrm{cm}^{-3}$, allows meaningful counting statistics to be obtained at these low temperatures.

The rf electric field in the poloidal direction is produced by a single turn, center tapped, Macor machinable ceramic clad, Faraday shielded antenna mounted in a retractable, rotatable fitting at the bottom center of the machine. The antenna structure also functions as a physical limiter. It forms the inductive

part of the oscillator tank circuit (Fig. 2) which determines the oscillator frequency ω. This contrasts with the conventional oscillator, amplifier, matching device, and antenna chain, where the rapidly changing loading reactance must be dynamically tuned out to prevent loss of efficiency. Any plasma reactance only shifts the oscillator frequency. The maximum $\Delta f/f_0$ is 0.6% for $\bar{n} = 6 \times 10^{12}$ cm^{-3}. The oscillator readily adjusts to the new parameters without loss of efficiency, but with substantial enhancement of the coupling to modes. The oscillator efficiency is kept high by maximizing the unloaded Q ($\approx$120) and hence the antenna circulating current. It is normally tuned to 12 MHz without plasma and can supply up to 1.2 MW of rf power to the tank circuit for a pulse length of 1.1 ms.

Since the rf source is not detuned enough by the plasma reactance to significantly alter its operating parameters, the plasma loading may be obtained by comparison of the oscillator d.c. drive current $I_{d.c.}$ with and without plasma. Calibration is performed using discrete non-inductive resistors placed across the antenna terminals. The instantaneous frequency shift is measured with a phase locked loop circuit (Biddle, 1980).

The Faraday shield reduces two major related problems. While the bulk of the plasma is naturally shielded from the large electrostatic fields generated near the antenna, these fields do accelerate particles at the plasma edge into the antenna with energies $\leq$20 keV. This bombardment results in high levels of impurities being injected into the plasma. The energy required for this sputtering, combined with that needed to excite electrostatic edge modes (Bernstein and Trehan, 1960), represent a significant loss unrelated to rf ion heating. It also complicates

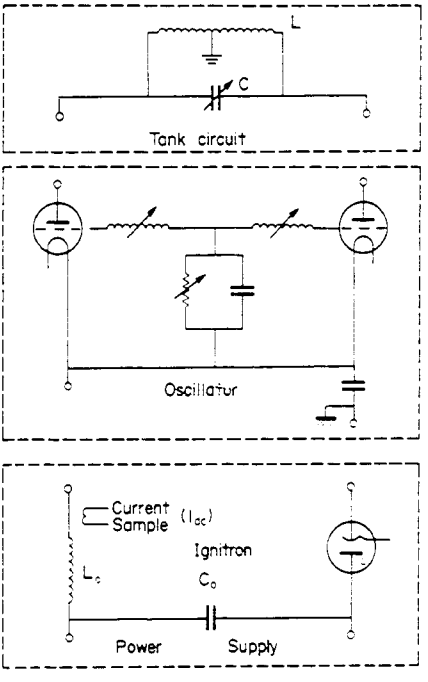

Fig. 2.—RF source and power supply. The antenna forms the inductor in the frequency determining tank circuit.

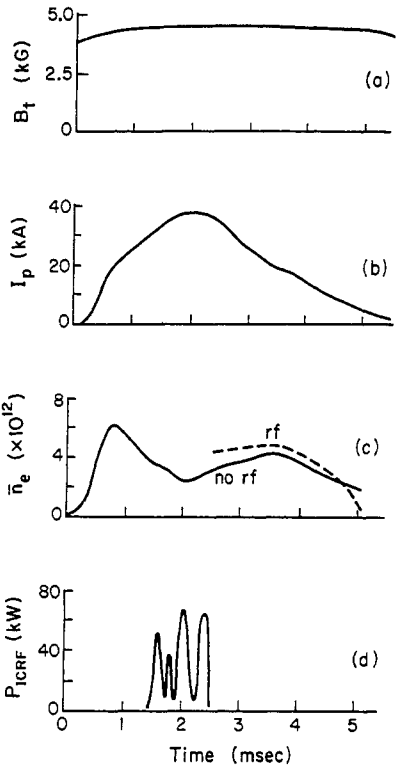

FIG. 3.—Typical time evolution of experimental parameters.

data analysis. The power represented by this 'parasitic' loading has been approximately accounted for in power deposited in the divertor in DIVA (KIMURA *et al.*, 1979). The installation of a Faraday shield over the Macor ceramic covering the antenna reduces the total 'parasitic' and actual power to the ions to 0.5 MW.

Figure 3 shows the typical time evolution of the experiment. The toroidal field is crowbarred and is essentially constant throughout the experiment (Fig. 3a). The plasma current (Fig. 3b) rises quickly and is constant for ≈ 1 ms during which the heating experiment is carried out. The density (Fig. 3c) is maintained by supplementary gas puffing, but it is only high enough to support normal eigenmodes from 0.5 to 2.0 ms. The ICRF power to the ions alone is shown in Fig. 3d. Not shown are a continuous 100 W, 2.45 GHz microwave source and a 10 kW, 9 GHz, 1 ms source triggered 0.5 ms before the ohmic heating voltage. These sources provide a cold, $T_e \approx 5$ eV, $n_e \approx 10^{10}$ cm^{-3} target plasma (SPROTT, 1969) for the ohmic heating. This reduces the loop voltage during startup (HOLLY *et al.*, 1980), reduces X-ray production from runaway electrons, and enhances shot-to-shot reproducibility.

The rf field measurements are made with a hollow 0.64 cm diameter stainless steel probe with a Macor tip which protects the 4-turn search coil. With proper cleaning, the search probe does not effect either the gross discharge properties or the independently measured plasma loading. An additional probe does not perturb the field structures.

3. EIGENMODE STRUCTURES AND HEATING THEORY

Probe measurements show that for propagation purposes the antenna effectively limits the high particle density current channel to a 13 cm radius with a low density, weakly ionized, evanescent region surrounding it. The current channel may be visualized as a dielectric waveguide since the conducting walls are located effectively at infinity. The conducting rings introduce some field distortion, but the current channel is still approximately cylindrically symmetric. The eigenmode structures are essentially those studied by LEHAN and PAOLONI (1972). At the period of highest density, both the $m=0$ and $m=+1$ modes are observed. Below the normal propagation cutoff density, (PAOLONI, 1975) the low density version of the $m=+1$ mode is observed. Theory shows this mode is largely left-hand circularly polarized (LHCP) near the plasma edge and right hand circularly polarized (RHCP) near the center. The reverse is true of the normal $m=+1$ mode. When rf is applied during the startup phase of the Tokamak, it produces excessive edge heating and impurity influx since the current and density profiles are hollow. The evanescent region surrounding the plasma requires the antenna to be as close as possible to the current channel (Fig. 4) to sample the maximum rf field flux.

We calculate the theoretical absorbed power from

$$\frac{P_{\text{icrh}}}{\text{unit volume}} = \frac{\sqrt{(\pi^2_{\text{pi}})k_1^2}}{4\omega_{ci}k_{\|}} v_t \exp\left[-\left(\frac{\omega-2\omega_{ci}}{k_{\|}v_t}\right)\right] |E_{\text{LHCP}}|^2$$

(SCHARER, MCVEY and MAU, 1977) with measured field values, thus bypassing the complicated edge region wave-antenna coupling. We have made the usual assumption that E_{LHCP} is constant over a vertical strip of width where the

$$\Delta X = \frac{k_{\|}v_t R}{\omega_{ci}}$$

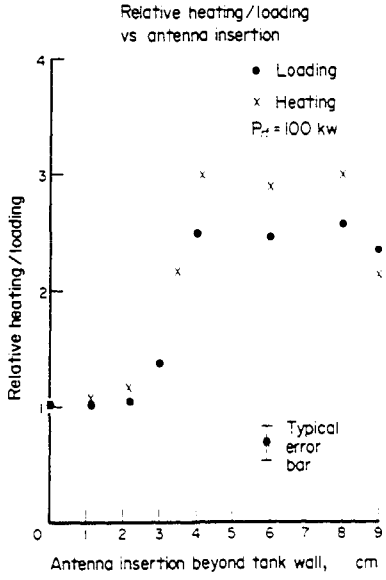

FIG. 4.—Relative heating and loading vs antenna insertion beyond tank wall. The approximately 13 cm region between the wall and the current is evanescnet and requires the antenna to be near the discharge for tightest coupling.

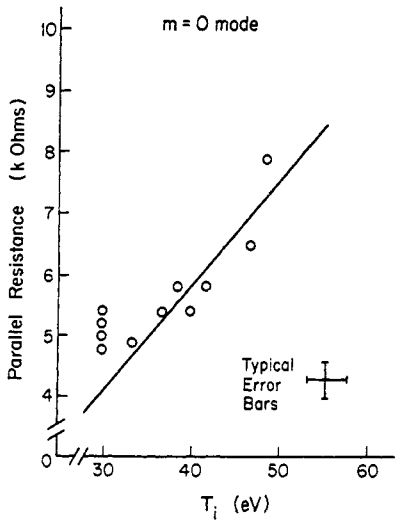

FIG. 5.—Measured rf power input vs theoretical power input. Higher loading is achieved with the $m = 0$ modes.

heating is appreciable. Here ω_{pi} is the ion plasma frequency, ω_{ci} is the ion cyclotron frequency, ω is the driving frequency, R is the major radius, v_{t_i} is the ion thermal velocity and $k_\perp$ and $k_\parallel$ are the wavenumbers perpendicular and parallel to the magnetic field, respectively. This is compared with the input power measured at the oscillator (Fig. 5). The agreement is within experimental error. The consistently higher than predicted loading is probably because of the crude rf field profile assumption which ignores the effects of the rings and the simplified density profile which neglects the plasma in the edge region. For a given mode, the effective parallel loading resistance at resonance rises with increasing ion temperature (Fig. 6) as expected. No changes in the loop voltage occurs at any

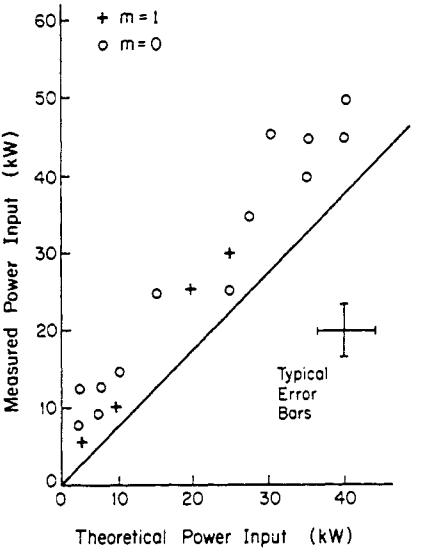

FIG. 6.—Parallel loading resistance vs ion temperature. The decline in power input with increasing temperature is characteristic of resonant mode effects.

radius with the application of rf, indicating that rf electron heating does not occur. This is as expected since the electron thermal velocity is only approximately 25% of the wave phase velocity, much too low for Landau or transit-time damping to be effective, even in the center of the plasma. The loop voltage does rise at late times with the influx of impurities.

4. PASSIVE MODE TRACKING

The similarity of a toroidal plasma eigenmode to a resonant cavity has long been known (STIX, 1975), and the large reactance imposed by an off resonance condition has been regarded as in impediment to efficient coupling (HWANG and GOULD, 1980). The same reactance, if applied to an oscillator such as in Fig. 2, will be shown to prove a limited passive mode tracking capability (see Section 2) with enhanced power deposition.

Following STIX (1975), we model the plasma series impedance imposed on the antenna structure by an individual eigenmode as

$$Z_{\text{total}} = Z_0 \frac{\sinh(a) + i \sin(b)}{\cosh(a) - \cos(b)} = r_s + iX_p$$

where a is the attenuation of the wave in one transit of the torus, and b is the phase shift ($b = 2\pi n$ where n is the number of parallel wavelengths around the torus). For a small device, the modes permitted are well separated in frequency. The other modes present thus contribute a relatively constant additional reactance which serves only to shift the effective unloaded oscillator frequency ω_0. Z_0 is a real coefficient chosen so the Z_{total} is the purely real loading obtained on a mode when n is integral. Z_{total} is computed in the usual manner (ADAM and JAQUINOT, 1977) for the specific antenna, plasma characteristics, and heating mechanism, or it may be measured directly.

Adopting the 'elliptical' approximation (TAKAHASHI, 1979) for the fast wave dispersion relation

$$N_\perp{}^2 + N_\parallel{}^2(\omega/\omega_{ci} + 1) = 0$$

where $N_\perp \equiv v_a/v_\perp$ and $N_\parallel \equiv v_a/v_\parallel$ are the Alfvén indices of refraction and v_a is the Alfvén velocity, we derive

$$b = 2\pi n' \left[\frac{\omega}{\omega'} \left(1 + \frac{\omega'}{\omega_{ci}} \Big/ 1 + \frac{\omega}{\omega_{ci}} \right)^{0.5} - 1 \right]$$

ω' is the frequency which represents the instantaneous mode center for a given density and profile, i.e. the toroidal mode number $n = n'$ an integer if $\omega = \omega'$, and ω is the actual oscillator frequency including the plasma reactive frequency shift. The instantaneous oscillator frequency is

$$\omega = \omega_0 \left[\frac{X_p}{2X_0} + \left(\frac{X_p{}^2}{4X_0{}^2} + 1 \right)^{0.5} \right].$$

We assume that the change in the dispersion relation is due to changes in the density rather than the magnetic field and that n' is much larger than the radial mode number. Both conditions are well satisfied here, but the latter will not be in

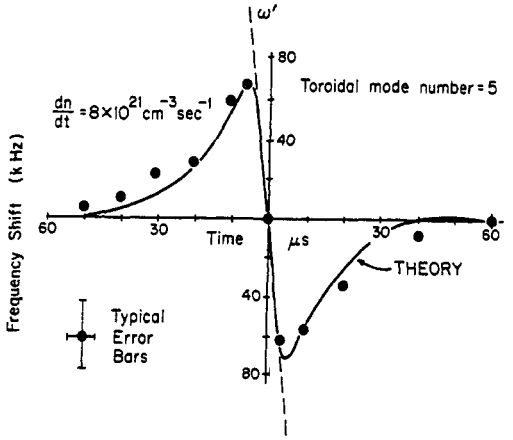

FIG. 7.—Plasma induced rf source frequency shift showing mode tracking. Tracking is greatest near the mode center.

a larger machine. The previous two equations are combined with the plasma reactance X_p and solved numerically to get the actual instantaneous frequency ω.

Using the typical values $a = 0.2$, $n = 5$, $X_0 = 50$, and $Z_{\text{total}} = 0.5$ ohms, we can show the theoretical agreement of the frequency shift in Fig. 7. The agreement is good within experimental error over a complete mode passage. The tracking range is enhanced by minimizing the antenna inductance while maximizing the ion loading. Figure 8 shows a theoretical calculation for the enhancement in power deposition by the use of passive mode tracking assuming the density changes at a constant rate during the mode passage. For this calculation, we have assumed a complete passage from antimode to antimode (i.e. n changes from $n'-0.5$ to $n'+0.5$). This gives a conservative result. The actual tracking is only strong near the mode center. This technique is ideal for small experiments. A reactor scale device with a high density of modes will not require great frequency excursions. This same proximity of other modes will, however, degrade the individual

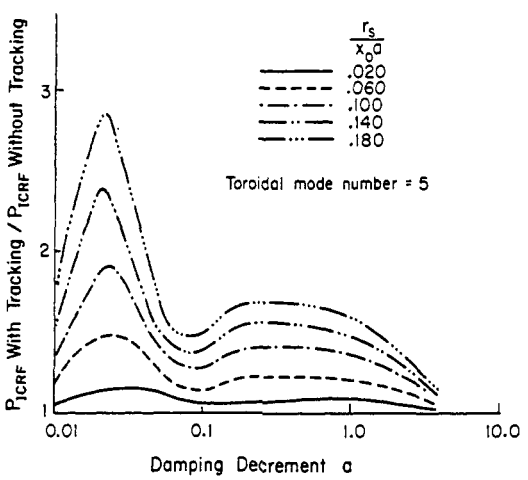

FIG. 8.—Enhancement of power deposition by mode tracing vs damping decrement.

tracking somewhat. Also, the strong minority damping found in a deuterium–tritium plasma may completely absorb the wave in one transit.

5. ION HEATING AND SCALING

An example of the ion distribution function as determined by charge exchange is given in Fig. 9. For 70 kW of rf absorbed by ions, with $I_p \approx 33$ kA, the body temperature increases from 35 to 75 eV. This temperature must be regarded with caution as the data come from the tail of the body distribution where instrumental statistics are rather poor. The high energy tail comprises ≈8% of the particles with a temperature of ≈320 eV. The partial cutoff beyond the gyroradius limit near 2 keV is associated with the poorly confined banana orbits (Rome *et al.*, 1976) due to the relatively low poloidal flux. Since the various segments of the distribution function are not well defined, it is probably more meaningful to speak of the average ion energy $\langle E \rangle$. This is increased from 40 to 115 eV representing an increase of approximately 1 eV per kW of rf.

The body and tail temperatures both tend to saturate with increasing ICRF power (Fig. 10). The collisonless particles in the tail are lost to the antenna structure (Kieras and Skinner, 1979) and to the copper rings. This latter effect is verified by an approximately 15 fold increase in line average CuI radiation with the application of rf in contrast to a doubling of the other impurities, mostly carbon, oxygen, and nitrogen. The body temperature, however, is evidently dominated by charge exchange loss due to the high neutral density caused by the low central electron temperature, ≈50 eV with the antenna inserted, and the small physical size of the device. Only factor of two estimates of the absolute charge exchange power loss can be made in the absence of detailed profile data, however. The highest temperatures are achieved with the minimum neutral filling pressure necessary for a stable, high current, discharge.

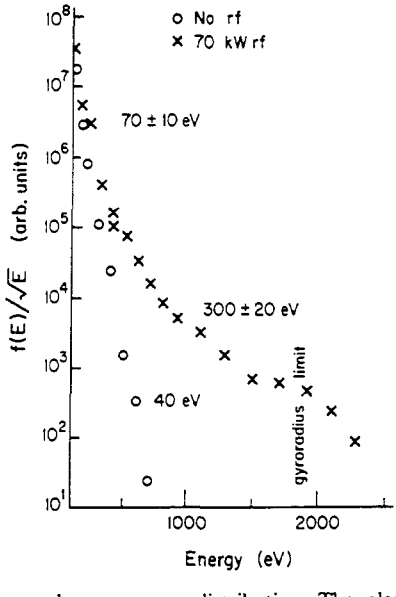

Fig. 9.—Typical charge exchange energy distribution. The plasma energy content is approximately trippled with 70 kW rf.

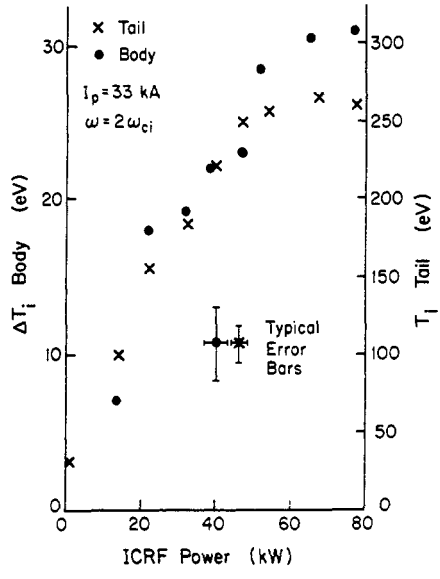

FIG. 10.—Tail and body temperatures vs rf power.

Significant ion heating occurs at cyclotron harmonics above $2\omega_{ci}$. With sufficient power to overcome the coupling inefficiency, and the discharge parameters held approximately constant, the attainable temperature saturates at approximately the same level (Fig. 11), independent of ω/ω_{ci}. The sole exception occurs with $\omega/\omega_{ci} = 1.5$ located on the minor axis. Tokapole II's geometry places the ω_{ci} and $2\omega_{ci}$ resonances beyond the inner and outer edges of the plasma column, respectively, resulting in negligible heating at any power level. This is consistent with the loss mechanism being independent of the heating mechanism. At lower

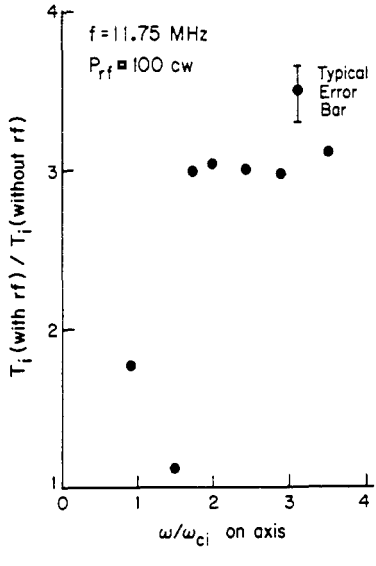

FIG. 11.—T_i (with rf)/T_i (without rf) vs ω/ω_{ci} on the axis at higher power. With sufficient power, the temperature saturates at about the same temperature.

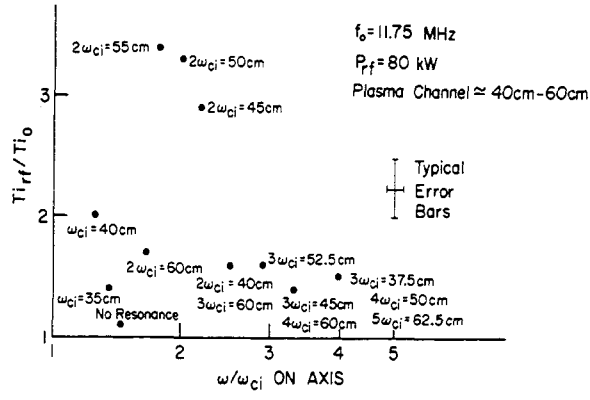

FIG. 12.—T_i (with rf)/T_i (without rf) vs ω/ω_{ci} on axis at medium power. At a low enough power input, the differennt coupling efficiencies are visible.

power levels, the heating produced with varying coupling efficiencies at higher harmonics becomes visible (Fig. 12). The 8 kG maximum toroidal field is only sufficient to place the fundamental resonance directly over the antenna rather than allowing launching from the propagating high field side. There are no significant effects noted from the resonance zone intersecting the antenna structure. The increase in temperature, even without optimization of the antenna structure, is apparent.

The relatively low efficiency of this ICRF system (Fig. 13) is due to the engineering compromises such as the antenna size and location required for compatability with other experiments and the lack of space for a completely effective Faraday shield, rather than any inherent limitations. The antenna subtends a poloidal angle of 30°, which results in the $m = 0, \pm 1$ Fourier coefficients being approximately 0.08.

The effect of increasing temperature on the ion energy confinement time t_i is seen in Fig. 14. At the highest currents the dominant loss mechanism is charge exchange, while at the lower currents the finite gyroradius effects become progressively more important. The improvement in scaling with plasma current is caused by both the better confinement of energetic ions and the increase in the size of the current channel. This result underlines the unsuitability of doing highly relevant high temperature confinement scaling studies in small devices, though the study of coupling and heating is quite profitable. The confinement scaling should be

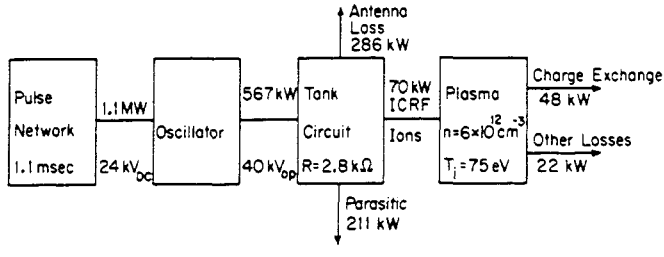

FIG 13.—RF power flow of experiment.

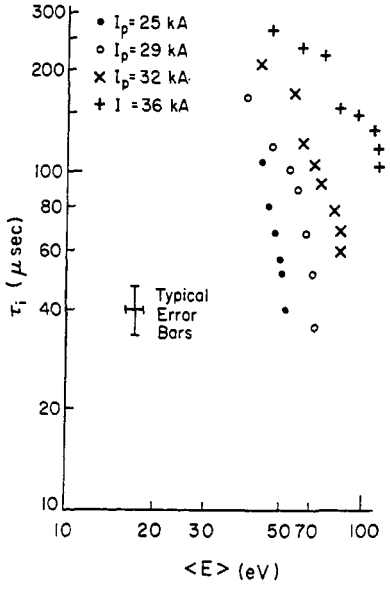

FIG. 14.—Ion energy confinement time vs ion average $\langle E \rangle$. The decrease in confinement time with increasing temperature is consistent with charge exchange and finite gyroradius effects being the dominant loss mechanisms.

improved markedly with more normal machine parameters. The thermal conduction loss should become relatively more important with higher ion and electron temperatures.

6. CONCLUSIONS

We have demonstrated that substantial body and tail heating can be obtained in a single ion species plasma by cyclotron harmonic heating in a Tokamak with poloidal divertors. Warm plasma theory including the large vacuum region surrounding the plasma has been shown to describe the heating well for the $m = 0$ and $m = +1$ modes. Ion temperatures have been more than doubled with the production of significant tails with no important deleterious effects from the enhanced impurity influx. Passive mode tracking is very effective in enhancing power deposition in low radial mode number eigenmodes and should work equally well in a larger device with proper preselection of $k_{\|}$ and an extension of the theory to higher radial mode numbers.

Significant ICRF heating, approximately a 50% increase in ion temperature without extensive optimization, occurs at the second, third and fourth of the ion cyclotron frequency.

Acknowledgements—Assistance from R. N. DEXTER on the spectroscopic measurements has been very helpful. The technical ssistance from B. KOLNER, T. LOVELL, P. NONN, A. SWENSON and R. VALLEM in designing and constructing the rf source and the launching structure made this research possible. We also gratefully acknowledge support from the U.S. Department of Energy.

REFERENCES

ADAM J. and JAQUINOT J. (1977) EUR-CEA-FC-886.
BIDDLE A. (1980) Ph.D. Thesis, University of Wisconsin.
BIDDLE A., DEXTER R., GROEBNER R., HOLLY D., LIPSCHULTZ B., PHILLIPS M., PRAGER S. and SPROTT J. (1979) *Nucl. Fusion* **9,** 1509.
BERNSTEIN I. and TREHAN S. (1960) *Nucl. Fusion* **1,** 3.
GROEBNER R. (1979) Ph.D. Thesis, University of Wisconsin.
HOLLY D., SHEPARD D., PRAGER S. and SPROTT J. (1981) to be published.
HOSEA J. and HOOKE W. (1973) *Phys. Rev. Lett.* **31,** 150.
HWANG D. and GOULD R. (1980) *Physics Fluids* **23,** 614.
KIERAS C. and SKINNER D. (1979) *Bull. Am. Phys. Soc.* **24,** 1062.
KIMURA H., ODAJIMA K., SENGOKU S., IIZUKA S., SUGIE T., TAKAHASHI K., YAMAUCHI T., KUMAGAI K., TAKEUCHI H., MATSUMOTO H., MATSUDA T., OHASA K., NAGAMI M., YAMAMOTO S., NAGASHIMA T., MAEDA H. and SHIMOMURA Y. (1979) Japan Atomic Energy Research Institute, JAERI-M 8429.
LEHAN J. and PAOLONI F. (1972) *Plasma Physics* **14,** 701.
LIPSCHULTZ B., PRAGER S., OSBORNE T., SPROTT J and PHILLIPS M. (1979) *Phys. Rev. Lett.* **43,** 36.
PAOLONI J. (1975) *Physics Fluids* **13,** 1570.
ROME J., MCALEES D., CALLEN J. and FOWLER R. (1976) *Nucl. Fusion* **16,** 55.
ROTHMAN M., SINCLAIR R., BROWN I. and HOSEA, J. (1969) *Physics Fluids* **12,** 2211.
SCHARER J., MCVEY B. and MAU T. (1977) *Nucl. Fusion* **15,** 297.
SPROTT J. (1969) Ph.D. Thesis, University of Wisconsin.
STIX T. (1975) *Nucl. Fusion* **15,** 737.
TAKAHASHI H. (1979) Princeton Plasma Physics Laboratory Report PPPL-1545.
VDOVIN, V. ZINOV'EV, O., IVANOV A., KOZOROVITSKII L., KROTOV M., PARAIL V., RAKHIMBABAEV YA., RUSANOV V. and SHAPOTKOVSKII M., (1973), *Sov. Phys. JETP Lett.* **17,** 2.